Supplementary Information

Singlet oxygen in non-aqueous oxygen redox: direct spectroscopic evidence for formation pathways and reliability of chemical probes

Soumyadip Mondal,[a] Rajesh B. Jethwa,[a] Bhargavi Pant,[a] Robert Hauschild,[a] Stefan A. Freunberger,*[a]

[a] Institute of Science and Technology Austria (ISTA), Am Campus 1, 3400 Klosterneuburg, Austria

Supplementary Methods

Generation of DMA-O_2. DMA reacts with $^1O_2$ to form DMA-O_2. $^1O_2$ was generated photochemically by illuminating O_2 saturated solutions containing 1 µM of the photosensitizer palladium(II) *meso*-tetra(4-fluorophenyl)tetrabenzoporphyrin (Pd_4F) at a wavelength of 643 nm in presence of DMA.[1]

Electrochemical oxidation of DMA. The electrosynthesis was done in a custom-made H-cell. The cathodic compartment consists of Pt working electrode with 5mL of 2mM DMA solution in 10 mM $KClO_4$ in acetonitrile. The anodic compartment consists of Ni foam as counter electrode with 5 mL of 100 mM 1,4-benzoquinone solution in acetonitrile. The two compartment was separated by K^+ selective ion-exchange membrane. Partially de-lithiated $Li_{(1-x)}FePO_4$ (MTI corporation) was used as reference electrode in the cathodic compartment. DMA was oxidized by galvanostatic charging until 80% of the total capacity was reached.

Supplementary Figures

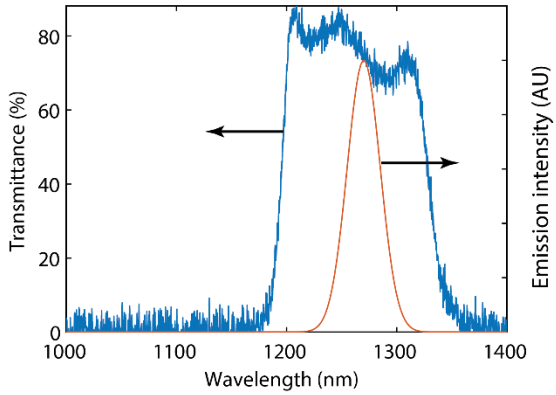

Fig. S1 Transmission data of the bandpass filter used for chemiluminescence from singlet oxygen ($^1O_2$) and simulated $^1O_2$ NIR emission at 1270 nm based on literature report.[2, 3]

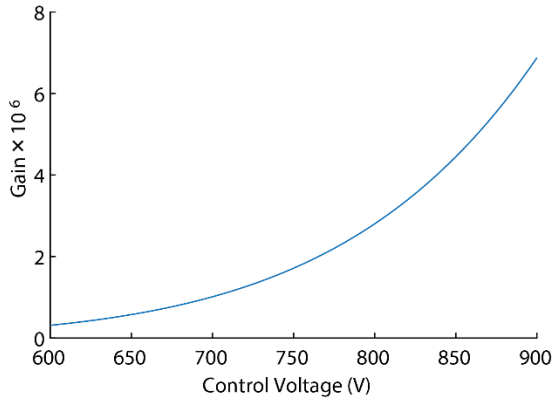

Fig. S2 Gain of the PMT detector vs control voltage. All signals from the PMT detector are normalised at a gain of 600 V control voltage.

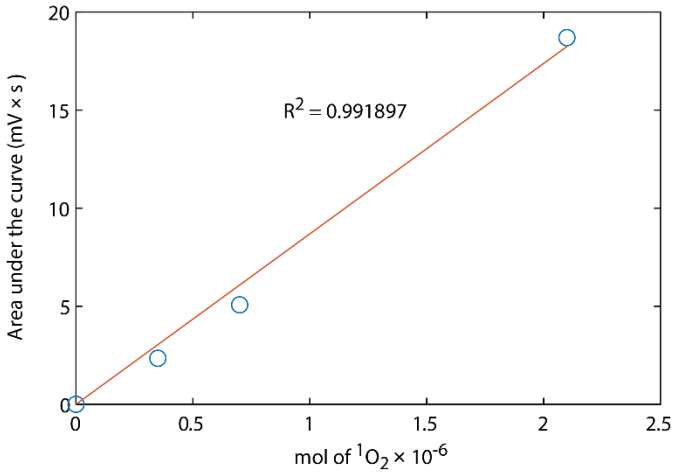

Fig. S3 Comparison of the area under the curve found from an output signal, to the amount of $^1O_2$ expected from the aqueous reaction of H_2O_2 and NaOCl.

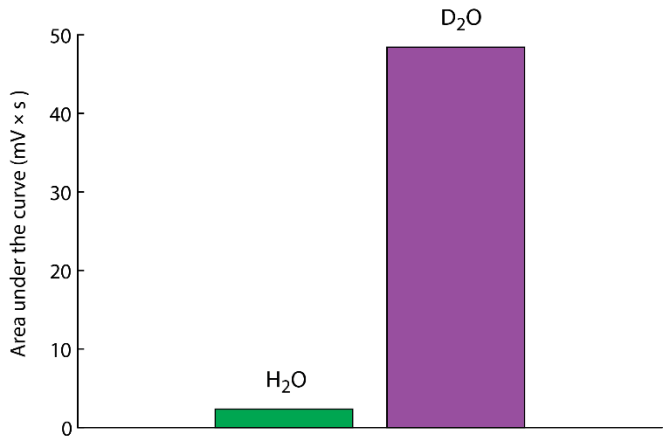

Fig. S4 Comparison of the area under the curve found from the output signal with the same concentration of H_2O_2 and NaOCl in H_2O and in D_2O. The difference between the areas under the curve is comparable between the difference in lifetime of $^1O_2$ in H_2O and D_2O.[4]

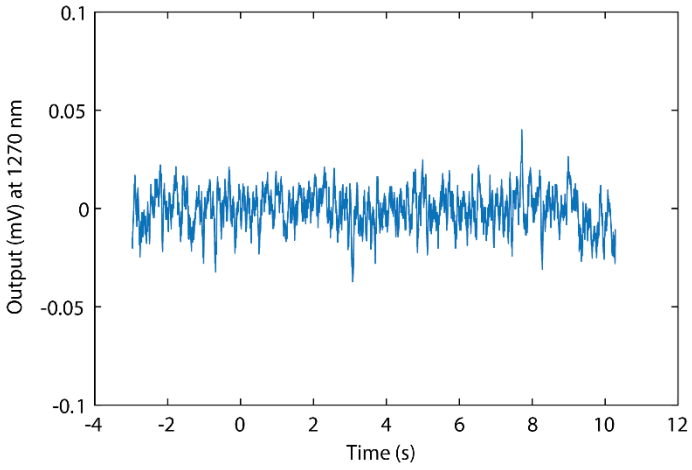

Fig. S5 Output signal upon injecting TBA^+ solution into a KO_2/crown ether (50 mM) suspension in acetonitrile. The time axis is relative to the injection time of the TBA^+ solution. The output signal is normalised at a gain of 600 V (control voltage).

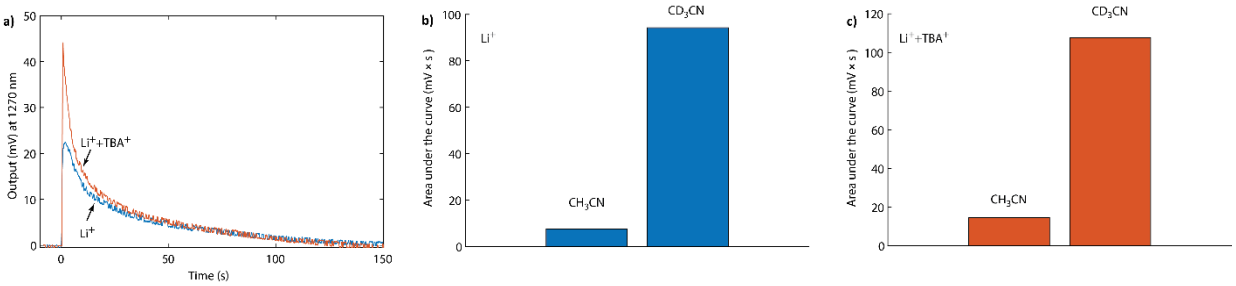

Fig. S6 (a) Superoxide disproportionation and signal from $^1O_2$ formation vs time upon disproportionation of a KO_2/crown ether (50 mM) suspension in acetonitrile-d3 in the presence of a Li^+-containing electrolyte or an electrolyte with 1:9 Li^+:TBA^+. The time axis is relative to injection time of the electrolyte solution. (b) and (c) Increase in the output signal as a function of area under the curve upon $^1O_2$ generation from superoxide disproportionation in acetonitrile and acetonitrile-d3. The increase in the area under the curve is comparable with the increase in lifetime of acetonitrile and acetonitrile-d3.[5] The output signal is normalised at a gain of 600 V (control voltage).

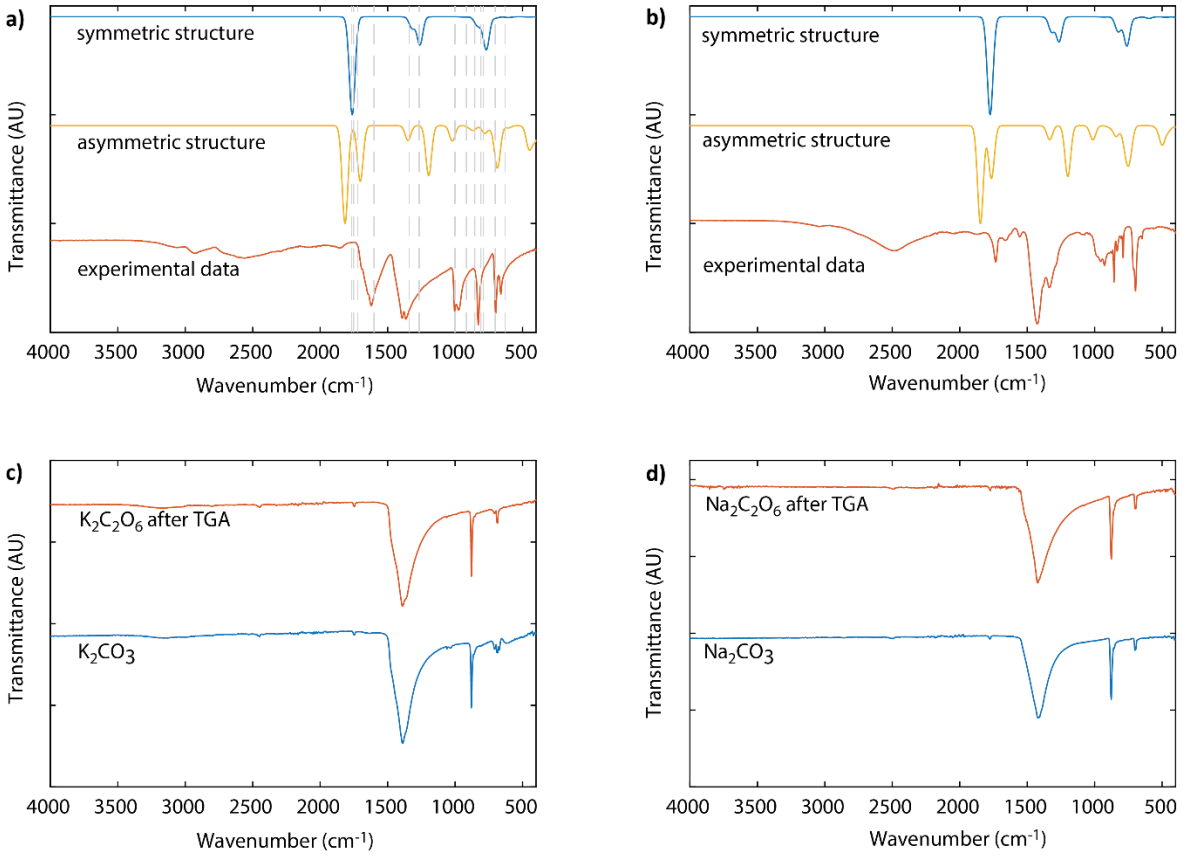

Fig. S7 Infrared spectroscopy of potassium peroxodicarbonate (a) and sodium peroxodicarbonate (b) with DFT calculated IR spectra for both symmetric and asymmetric metal peroxodicarbonates. The grey dashed lines in (a) correspond to literature reference frequencies for symmetric potassium peroxodicarbonate from ref 6. Infrared spectroscopy of potassium peroxodicarbonate (c) and sodium peroxodicarbonate (d) after TGA compared to the spectra of the analogous metal carbonates.

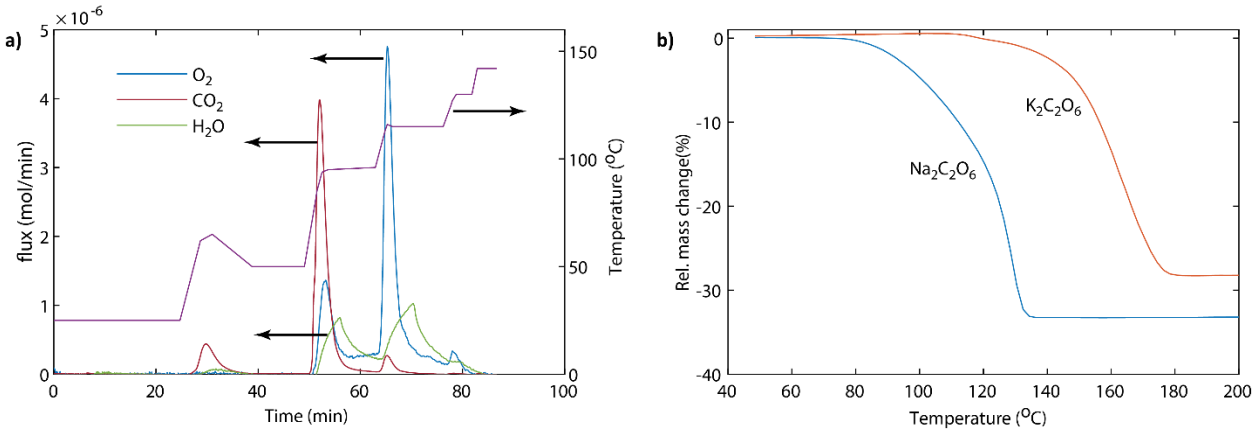

Fig. S8 (a) CO_2, O_2 and H_2O evolution from mass spectrometry on heating sodium peroxodicarbonate at different temperature steps indicating peroxo- bond decomposition and crystalline water removal. (b) Relative mass change (%) vs temperature from TGA. The convoluted mass change is a mixture of CO_2, O_2 and H_2O loss as indicated by mass spectrometry.

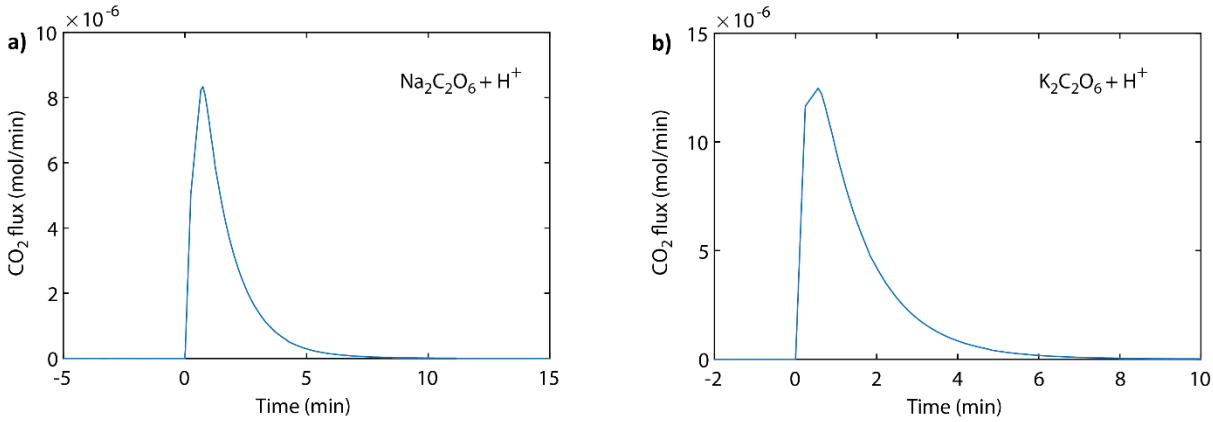

Fig. S9 CO_2 evolution as measured by mass spectrometry upon adding sulphuric acid to the synthesised metal peroxodicarbonates. The time axis is relative to the injection time of acid.

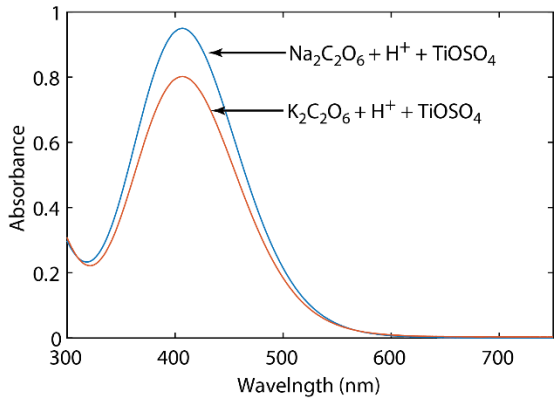

Fig. S10 Measuring the peroxo- content in the synthesised metal peroxodicarbonates via UV-Vis spectroscopy after treating the sample with $TiOSO_4$ in sulphuric acid.

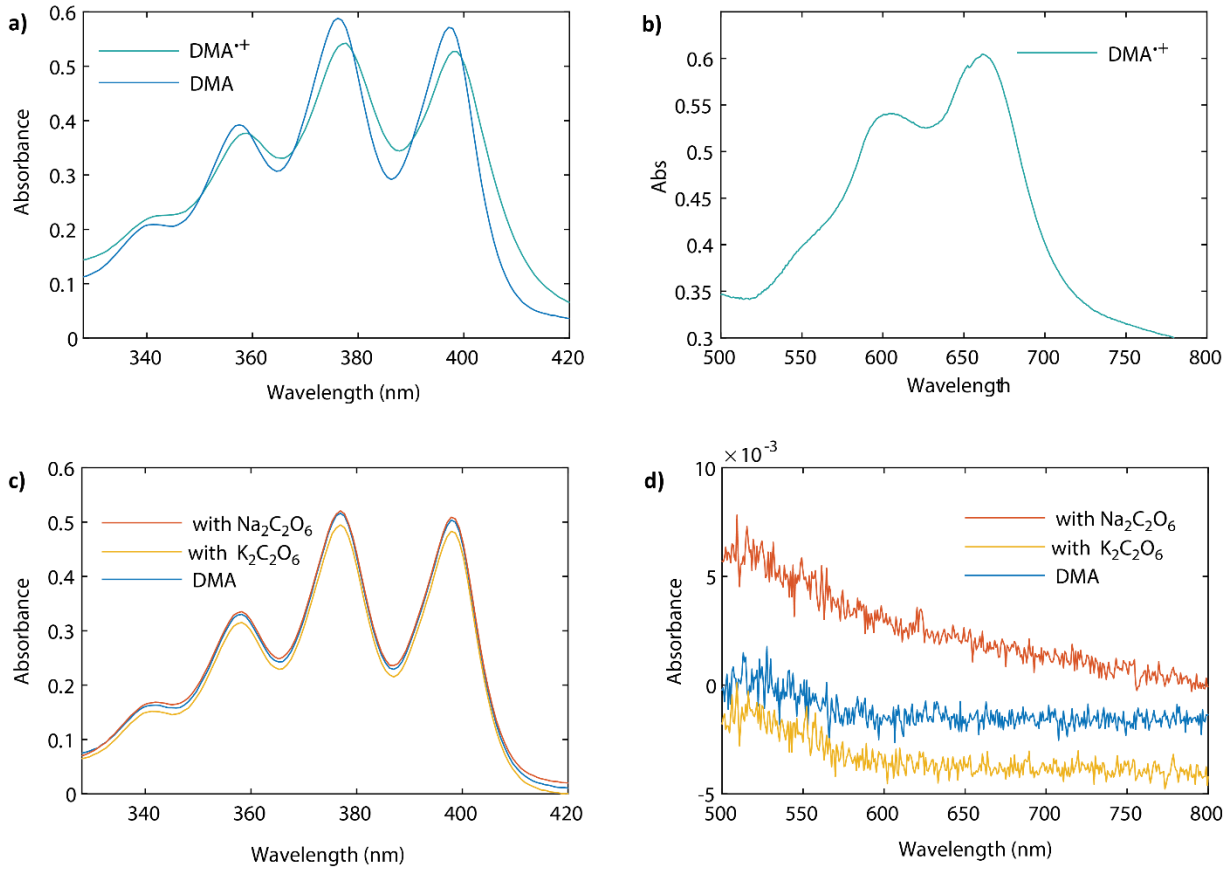

Fig. S11 (a) UV-Vis spectra of DMA and $DMA^{\bullet+}$ in the UV region. (b) UV-Vis spectra of $DMA^{\bullet+}$ in the visible region. UV-Vis spectra of metal peroxodicarbonates in contact with DMA and DME together with reference spectra of DMA in the UV region (c) and visible region (d) of the electromagnetic spectrum. The combined concentration of DMA and $DMA^{\bullet+}$ in the solution was 0.07 mM (a & c) and 1.2 mM (b & d).

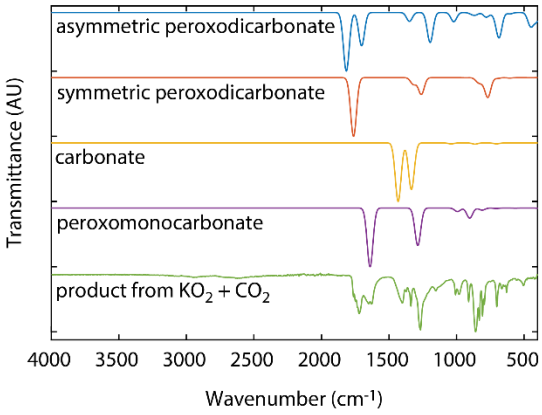

Fig. S12 FTIR spectra of the reaction product formed by purging CO_2 over KO_2 suspension in DME and computed IR spectra from DFT calculation for the symmetric and asymmetric potassium peroxodicarbonate, potassium peroxomonocarbonate and potassium carbonate. The FTIR spectrum of the reaction product indicates that it is a mixture of symmetric and asymmetric potassium peroxodicarbonate, potassium peroxomonocarbonate, and potassium carbonate as proposed in Fig 4a.

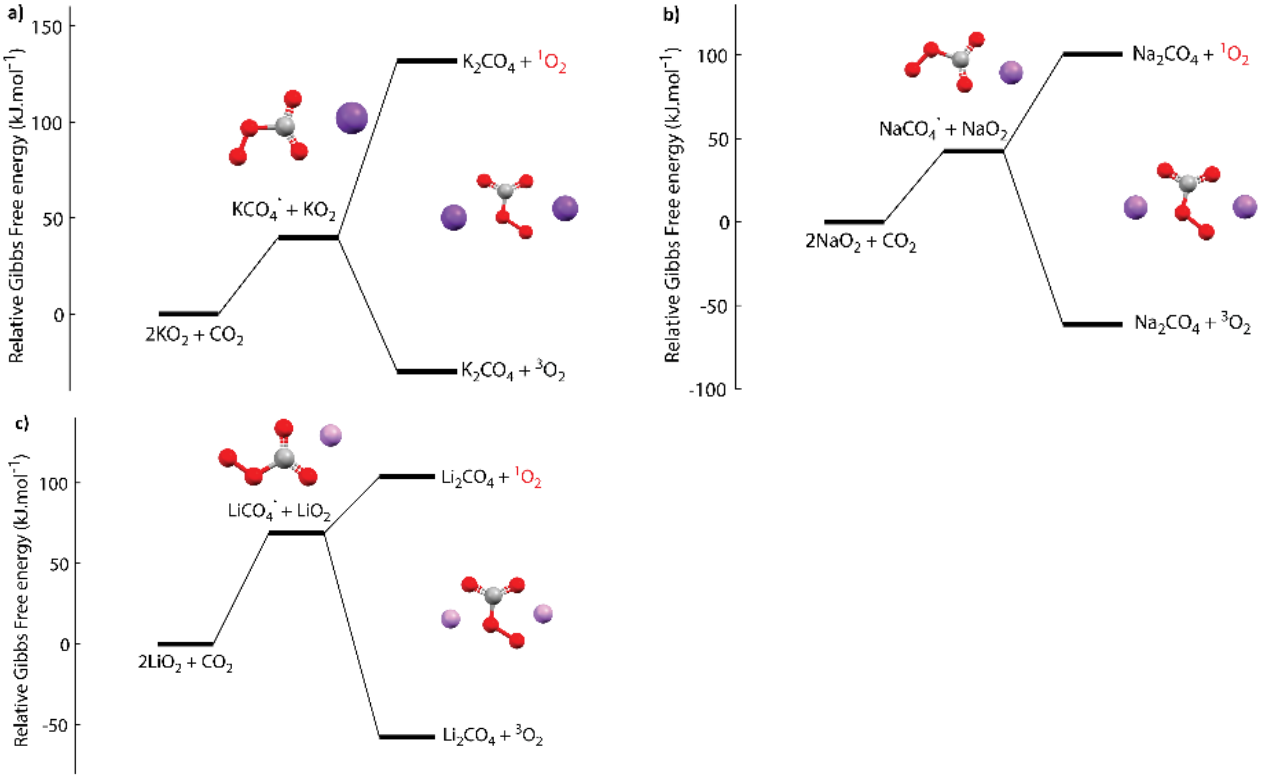

Fig. S13 Figure showing the relative energies calculated by DFT (B3LYP[7]/def2QZVPP[8-11], implicit DME solvation[12]) along the reaction coordinate in kJ·mol^{-1} of the potassiated (a), sodiated (b), and lithiated (c) peroxomonocarbonates and their respective proclivities towards $^1O_2$ vs $^3O_2$ release.

Table S1: Table listing the Gibbs Free Energies of the compounds used to calculate the reaction coordinates depicted in Fig. S13. The calculations were performed at the B3LYP[7]/def2QZVPP[8-11] level of theory with PCM[12] implicit solvation for DME applied.

Compound	Gibbs Free Energy / 10^8 kJ.mol^{-1}
$^1O_2$	-3.947510
$^3O_2$	-3.949126
CO_2	-4.954150
LiO_2	-4.148877
NaO_2	-8.212433
KO_2	-10.970291
$LiCO_4$	-9.102339
$NaCO_4$	-13.16616
KCO_4	-24.65666
Li_2CO_4	-9.303355
Na_2CO_4	-17.43050
K_2CO_4	-40.41113

DFT Coordinates

$^1O_2$

Element	x	y	z
O	-2.148528	1.708453	0.000000
O	-1.237432	0.923367	0.000000

$^3O_2$

Element	x	y	z
O	-2.148735	1.708632	0.000000
O	-1.237225	0.923188	0.000000

CO_2

Element	x	y	z
C	-0.287290	0.964487	0.000000
O	0.711232	1.552169	0.000000
O	-1.285812	0.376803	0.000000

LiO_2

Element	x	y	z
O	-2.305448	2.203401	0.000000
O	-2.104420	0.876448	0.000000
Li	-3.854962	1.283431	0.000000

NaO_2

Element	x	y	z
O	-2.093337	2.156081	0.000000
O	-2.031093	0.812800	0.000000
Na	-4.140400	1.394400	0.000000

KO_2

Element	x	y	z
O	-1.970745	2.143662	0.000000
O	-1.932028	0.805114	0.000000
K	-4.362047	1.414504	0.000000

$LiCO_4$

Element	x	y	z
O	-1.526632	1.051132	0.000020
C	-0.439830	1.647075	0.000002
O	1.862325	1.304535	-0.000010
O	0.685038	0.721004	0.000005
O	-0.230739	2.861216	-0.000016
Li	-2.182861	2.875087	-0.000001

$NaCO_4$

Element	x	y	z
O	-1.452123	0.975508	0.000002
C	-0.400704	1.623235	-0.000015
O	1.932069	1.305627	0.000031
O	0.766455	0.704818	-0.000012
O	-0.186810	2.831262	-0.000030
Na	-2.491577	3.019621	0.000025

KCO_4

Element	x	y	z
O	-1.387090	0.923099	0.000001
C	-0.359447	1.599293	0.000006
O	1.997616	1.283758	-0.000011
O	0.836875	0.677622	0.000002
O	-0.143158	2.803145	0.000012
K	-2.777486	3.173143	-0.000010

Li_2CO_4

Element	x	y	z
O	-1.414173	1.592253	-0.018136
C	-0.159210	1.484356	-0.006887
O	1.626205	-0.139756	0.021476
O	0.199800	0.150713	0.008018
O	0.718898	2.360603	-0.007509
Li	-1.675425	-0.257544	-0.004939
Li	2.350755	1.514566	0.007977

Na_2CO_4

Element	x	y	z
O	-1.400247	1.710383	0.063148
C	-0.152218	1.532222	0.041639
O	1.539938	-0.230334	-0.069988
O	0.142421	0.180608	-0.036066
O	0.752858	2.382293	0.080955
Na	-2.016488	-0.422482	-0.028584
Na	2.780575	1.552501	-0.051103

K_2CO_4

Element	x	y	z
O	-1.374261	1.815459	0.000233
C	-0.136351	1.561684	0.000141
O	1.477453	-0.249539	-0.000190
O	0.090591	0.199874	-0.000094
O	0.813926	2.363792	0.000233
K	-2.420199	-0.505194	-0.000233
K	3.195331	1.517392	-0.000089

Supplementary References

1. S. M. Borisov, G. Nuss, W. Haas, R. Saf, M. Schmuck and I. Klimant, *J. Photochem. Photobiol. A*, 2009, **201**, 128-135.
2. A. U. Khan, *Journal of Bioluminescence and Chemiluminescence*, 1989, **4**, 200-207.
3. J. Regensburger, T. Maisch, A. Felgenträger, F. Santarelli and W. Bäumler, *Journal of Biophotonics*, 2010, **3**, 319-327.
4. C. Schweitzer and R. Schmidt, *Chemical Reviews*, 2003, **103**, 1685-1758.
5. P. R. Ogilby and C. S. Foote, *Journal of the American Chemical Society*, 1983, **105**, 3423-3430.
6. P. A. Giguère and D. Lemaire, *Canadian Journal of Chemistry*, 1972, **50**, 1472-1477.
7. A. D. Becke, *The Journal of Chemical Physics*, 1993, **98**, 5648-5652.
8. A. Schäfer, C. Huber and R. Ahlrichs, *The Journal of Chemical Physics*, 1994, **100**, 5829-5835.
9. A. Schäfer, H. Horn and R. Ahlrichs, *The Journal of Chemical Physics*, 1992, **97**, 2571-2577.
10. F. Weigend, *Physical Chemistry Chemical Physics*, 2006, **8**, 1057-1065.
11. F. Weigend and R. Ahlrichs, *Physical Chemistry Chemical Physics*, 2005, **7**, 3297-3305.
12. G. Scalmani and M. J. Frisch, *The Journal of Chemical Physics*, 2010, **132**.